Sixth International Conference on
NANO-TECHNOLOGY IN
CONSTRUCTION
المؤتمر الدولى السادس لتكنولوجيا النانو فى الانشاء
(NTC 2014)
Housing & Building National Research Center
المركز القومى لبحوث الإسكان والبناء
(HBRC).
Egyptian -Russian University (ERU)
الجامعة المصرية الروسية
Izhevsk State Technical University (ISTU)

PHYSICAL PROPERTIES OF ZnO/PVA NANOCOMPOSITE FILMS

S. El-Sayed[1,2], W. M. Morsi[3], A. M. El Sayed[1,4] and A. Hassen[1,2]*

[1] Physics Department, Faculty of Science, Fayoum University, Fayoum 63514, Egypt.
[2] Physics Department, Faculty of Science and Education, Taif University, KSA.
[3] Housing and Building National Research Center, HBRC, Dokki, Giza, Egypt.
* dr.wafaam@yahoo.com
[4] Physics Department, Faculty of Science, Northern Borders University, Arar, KSA.

Abstract

Nano-sized zinc oxide (ZnO) was synthesized by sol-gel method, and mixed with polyvinyl alcohol (PVA) to produce nanocomposite films. X-ray diffraction (XRD) revealed that the average particle size of ZnO is about 26 nm and its original structure remains unaltered in the PVA matrix. Scanning electron microscopy (SEM) was used to observe the morphology and dispersion of ZnO on the surface of the PVA films. The results of differential scanning calorimetry (DSC) showed that both thermal stability and degree of crystallinity of pure PVA were reduced by the addition of ZnO nanoparticles. Dielectric constant (ε') and ac conductivity (σ_{ac}) of all samples were measured within temperature and frequency ranges of 300-468 K and 10 kHz-2 MHz, respectively. The behavior of $\sigma_{ac}(f)$ for pure PVA, as well as composite films indicated that the conduction mechanism was correlated barrier hopping (CBH). The results from this work were discussed and compared with those of previous studies of PVA composites.

Keywords: ZnO nanoparticles; Polyvinyl alcohol (PVA); X-ray diffraction; Dielectric and optical properties.

1. Introduction

Polymer-based nanocomposites is a subject of considerable research due to their ability to combine the advantages of both polymer and filler component. Based on their optical, electrical, mechanical and magnetic properties[1,2], there are several applications of polymeric nanocomposites. Many groups focus on dispersing metal oxide nanoparticles into polymer matrix[3-12]. It has been found that the physical properties of polymeric materials can be modified by metal oxide nanoparticles depending on composition, metal oxide concentration, particle size, and dispersion homogeneity.

Polyvinyl alcohol (PVA) has fascinating properties and a wide variety of applications because it has high dielectric strength and good charge storage capacity. Its optical as well as electrical properties depend on the type of doping filler. It has also gained increasing attention for biomedical applications[13]. PVA has a carbon chain backbone with hydroxyl groups, which can act as a source of hydrogen bonding to enhance the formation of polymer complexes[14]. Zinc oxide (ZnO) has received much attention because of its diverse properties. It has a direct wide band gap semiconductor ($E_g \approx 3.4$ eV) with large exciton binding energy[15]. It also exhibits strong ultraviolet[16] and visible photoluminescence[17]. With all these important properties, ZnO has many applications[18] such as: photo catalysis, gas sensors, varistors, and low-voltage phosphor material.

PVA is a semi-crystalline polymer, and its crystalline index depends on the synthetic process and physical aging[19]. The crystalline nature of PVA results from the strong intermolecular interaction of PVA chains through intermolecular hydrogen bonding. Typically, its maximum intensity diffraction peak is observed at $2\theta = 19.8^{\circ}$ corresponding to a *d*-spacing of 4.4801Å for the (101) crystal plane[20]. Two other peaks are also found around 22.9°, and 40.6° [21]. On the other hand, the crystal structure of ZnO is hexagonal with diffraction peaks corresponding to (100), (002), (101), (102), (110), (103), and (112) planes [9]. The lattice parameters are a = 3.2466 Å and c = 5.2044 Å [22].

Different research groups have investigated the structure, optical, and dielectric properties of PVA containing different dopants. The x-ray diffraction (XRD) results of zinc oxide/polyvinyl alcohol (ZnO/PVA) nanocomposite films revealed that the original structure of ZnO nanoparticles remained unaltered in the PVA matrix and they were uniformly distributed on the film surface[3]. However, the presence of ZnO in the PVA film caused changes in the optical properties of PVA, where UV-vis absorption band at 370 nm was observed. The addition of 0.5 wt.% ZnO nanoparticles to PVA was desirable for dielectric properties [23]. The addition of 0.1, 0.3, or 0.5 wt.% vanadium pentoxide (V_2O_5) nanoparticles to pure PVA changed its crystallinity due to the interaction between vanadium ions and the OH groups of PVA[8]. The effect of V_2O_5 nanoparticles on the dielectric properties of PVA has shown that the frequency dependence of the ac conductivity follows Jonscher universal dynamic law. Nano-sized NiO altered the structure, thermal and optical properties of PVA[24]. Graphite oxide nanoplatelets (GOnP) cause a significant increase in both the electrical conductivity and dielectric permittivity of PVA[10]. Furthermore, graphene (GE) based nanocomposites have been shown to improve the thermal stability, degree of crystallinity, and mechanical properties of PVA[25].

From the previous studies, the physical properties of metal oxides doped PVA are interesting due to their varied applications. In particular, introduction of ZnO filler into

polymer matrix can modify its optical and electrical properties [26,27]. In this work, we prepared and characterized ZnO nanoparticles to investigate their effect on the structure, thermal, and dielectric properties of PVA. The results were compared with those of previous reports on similar metal oxide/PVA composites.

2. Materials and methods

2.1. Preparation of ZnO nanoparticles

Zinc oxide (ZnO) nanoparticles were synthesized by a sol-gel method. High purity zinc acetate dehydrate $Zn(C_2H_2O_2.2H_2O)$ and oxalic acid ($C_2H_2O_4$) were mixed in stoichiometric ratio and dissolved in double distilled (DD) water under a magnetic stirring for two hours. The obtained sol was held in an oven at 100 °C for 8 h, cooled to 70 °C and stirred to obtain a gel that was then aged for 18 h at room temperature. Finally, the gel was calcined at 450 °C for 3 h to obtain ZnO nanoparticles.

2.2. Preparation of ZnO/PVA nanocomposite films

The synthesized ZnO nanoparticles were added in different ratios, *x* (wt.%; 0, 0.25, 0.50 and 0.75) to PVA according to:

$$x(\text{wt.}\%) = 100 \times \frac{w_f}{(w_f + w_p)} \qquad (1)$$

where w_f and w_p represent the weights of ZnO and PVA polymer, respectively. The nanocomposite films were prepared by casting as follows; 2.0 g PVA, (Avondale Laboratories, Banbury Oxon, England, average molecular weight of 17,000 GRG) was dissolved in 100 mL DD water at 90 °C and stirred for 3 h. ZnO nanoparticles were added to the PVA solution under vigorous stirring to prevent any agglomeration. Finally, the aqueous mixtures were cast into Petri dishes and placed in an oven at 60 °C for 24 h in air. The obtained nanocomposite films of pure PVA and PVA loaded with ZnO nanoparticles were characterized.

2.3. Experimental

Scanning electron microscopy (SEM; Inspect S, FEI, Holland) images were taken for pure PVA and the nanocomposite films. XRD of all samples was performed using a PANalytical's X'Pert PRO. Thermal analysis was carried out using a Shimadzu DSC-50 in the temperature range 32-250 °C with a heating rate of 10 °C/min. Dielectric measurements were performed by using a Hioki (Ueda, Nagano, Japan) model 3532 High Tester LCR, with a capacitance measurement accuracy on the order of 0.0001 pF. The temperature was measured with a *T*-type thermocouple having an accuracy of ±1 °C. The dielectric constant ε' of each sample was calculated as $\varepsilon' = dC/\varepsilon_0 A$, where *C* is the

capacitance, d is the thickness of the sample, ε_0 is the permittivity of free space, and A is the cross-sectional area of the sample.

3. Results and discussion

3.1. Characterization

Fig. 1 shows the XRD pattern of the ZnO nanoparticles. All the observed reflection peaks are consistent with previous reports[9,22]. The XRD peaks were indexed by a hexagonal structure as reported in JCPDS card No. 89-1397. From XRD, the particle size of the ZnO was calculated using Scherrer formula [9]:

$$L = \frac{0.9\lambda}{B\cos\theta} \qquad (2)$$

where L is the crystal size of the particle, λ is the wavelength of x-ray radiation (1.5406 Å), B is the full width at half maximum (FWHM) intensity expressed in radians and θ is the diffraction angle.

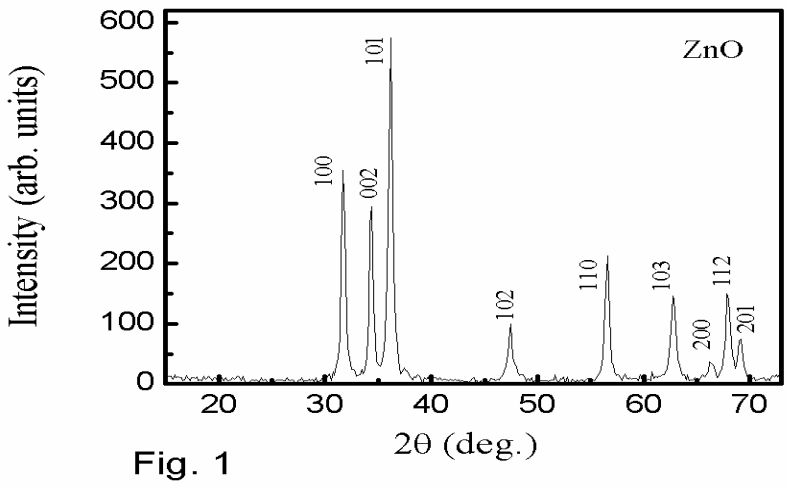

Fig. 1: XRD diffraction of ZnO nanoparticles at room temperature.

To throw light on the effect of ZnO nanoparticles on the structure of PVA, XRD of pure PVA and PVA mixed with ZnO nanoparticles were presented in Fig. 2(a-d). The observation of the maximum intensity diffraction peak of pure PVA at 2θ ≈ 19.51° corresponding to d spacing 4.5511Å, and reflection plane (101), consistent with earlier studies [20]. Another small peak observed around 2θ ≈ 40.6° indicated the presence of the typical semicrystalline structure of PVA (see Fig. 2(a)). For composite samples (Fig. 2(b-d)), these two peaks were also observed in addition to the peaks at 2θ ≈ 31.67, 34.31, 36.15 and 56.52° which correspond to the reflection planes of the ZnO[9] (see Fig. 1) and

consistent with those in previous report[3]. These reflections indicate that the original structure of the ZnO nanoparticles remains unaltered in the PVA matrix. ZnO nanoparticles ranged from 17 to 30 nm with an average 26 nm as given in Table 1.

Table 1: XRD data of ZnO nanoparticles; the full width at half maximum (FWHM), *L* is the calculated particle size according to Eq. 2.

2θ (deg.)	d-spacing (Å)	I/I_0 %	FWHM	*L* (nm)
31.67	2.8205	62.8	0.48690	29.6
34.31	2.6095	49.7	0.47734	30.4
36.15	2.4802	100	0.55785	25.9
47.44	1.9113	17.8	0.77666	19.5
56.52	1.6255	35.4	0.53362	29.5
62.75	1.4783	25.8	0.74839	21.7
66.29	1.4076	5.4	0.69288	23.9
67.85	1.3789	24.8	0.53558	31.2
69.01	1.3588	12.4	0.61406	27.4
72.44	1.3029	2.8	0.98774	17.4
76.87	1.2384	2.9	0.71087	24.9

One also noticed that the position of the maximum intensity peak of PVA changed very slightly with the addition of ZnO to PVA matrix. SEM was performed to examine the morphology and dispersion of ZnO nanoparticles on the surface of PVA films.

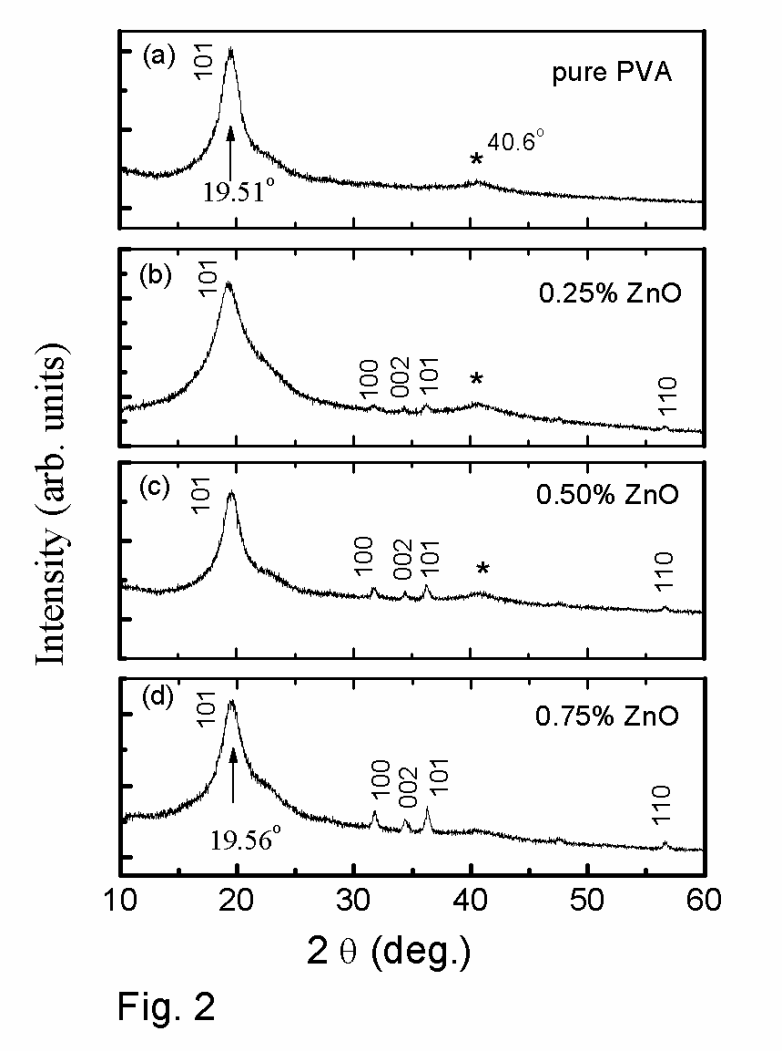

Fig. 2

Fig. 2: XRD patterns for: (a) pure PVA, (b) 0.25 wt.% ZnO-doped PVA, (c) 0.50 wt.% doped PVA, and (d) 0.75 wt.% doped PVA films.

Fig. 3 (a-c) displays SEM images for pure PVA and some selected ZnO/PVA nanocomposite films, in which it can be seen that there was a good dispersion of ZnO nanoparticles on the surface of the PVA.

Fig. 3: SEM for: (a) pure PVA, (b) *0.50* wt.% ZnO-doped PVA, and (c) 0.75 *wt.*% ZnO-doped PVA films.

3.2. Differentional scanning calorimetry (DSC)

DSC was carried out to determine phase transitions such as glass transition (T_g), crystallization (T_c) and melting (T_m) temperatures of the samples. Fig. 4 shows the DSC heating runs to 250 °C of pure PVA and PVA loaded with ZnO nanoparticles. Three endothermic peaks were distinguishable for pure PVA as indicated by arrows. The first peak observed at 50 °C was due to T_g of the α_a-relaxation process resulting from micro-Brownian motion of the main chain backbone[28]. The second peak ($T_{\alpha c}$), which was broad similar to that observed in Refs.[28,29], was attributed to the α_c-relaxation

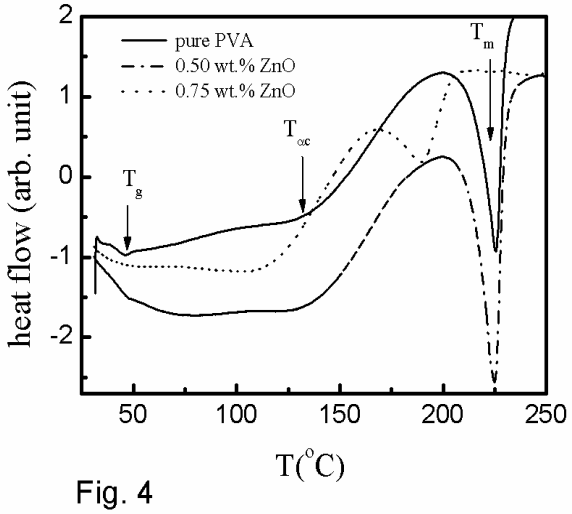

Fig. 4

Fig. 4: DSC thermogram for a heating rate of 10 °C/min for pure PVA film and PVA films loaded with 0.50 and 0.75 *wt.*% of ZnO nanoparticles. The arrows indicate the transition temperatures of pure PVA.

associated with crystalline regions. The third peak located at 226 °C due to the melting temperature T_m[19,24,30]. For the composite films, the first and second peaks became broad. The third peak, T_m, was found around 197, 225 and 191 °C for 0.25 (not shown here), 0.50 and 0.75 wt.% ZnO-doped PVA, respectively. This means that T_m shifts towards lower temperatures with ZnO addition to PVA. The observed change of T_m in ZnO/PVA composites was different compared to that found for Cr_2O_3/PVA nanocomposite films[31]. It can be suggested that the loading of PVA with different amounts of ZnO decreases its thermal stability, i.e., the PVA segments get soft with the incorporation of ZnO nanoparticles. The observed decrease of T_m indicated that segmental mobility of PVA increased and became less rigid with the addition of ZnO nanoparticles as in the case of $BaCl_2$ doped-PVA [28].

On the basis of the melting enthalpy, ΔH_m, the degree of crystallinity of pure PVA and the nanocomposite films were calculated as follows[32]:

$$X_c = 100 \times \frac{\Delta H_m}{\Delta H_0 X_m} \qquad (3)$$

where ΔH_0 is the heat of fusion of 100% crystalline PVA (138.6 J/g) [33] and X_m is the weight fraction of PVA in the composites. The values of T_m, ΔH_m and X_c% are given in Table 2. It is worthwhile to mention that the deviation in the values of both ΔH_m and X_c% of pure PVA film from those reported in Refs.[28,34] can be explained according to the different synthetic process, physical aging[19], purity, and average molecular weight of PVA used. Moreover, the crystallinity of the PVA was decreased by the incorporation of ZnO nanoparticles similar to that previously reported for NiO/PVA nanocomposites[24].

Table 2: Physical properties of pure PVA and PVA loaded with ZnO nanoparticles.

Composite films		T_m (°C)	ΔH_m (J/g)	X_c%
ZnO(%)	PVA(%)			
0	100	225.48	41.10	30
0.25	99.75	195.11	37.37	27
0.50	99.50	224.85	32.61	24
0.75	99.25	189.49	12.47	9

3.4. Dielectric properties

Fig. 5 (a-d) represents the frequency dependence of the real part of the dielectric constant, ε', for pure PVA and PVA loaded with ZnO nanoparticles at some selected temperatures. It was found that ε' decreased systemically with increasing frequency. This observed decrease of ε' with frequency for all samples at given temperatures may be attributed to a decreasing number of dipoles, which contribute to polarization or the dipole structure is no longer able to respond to the applied electric field.

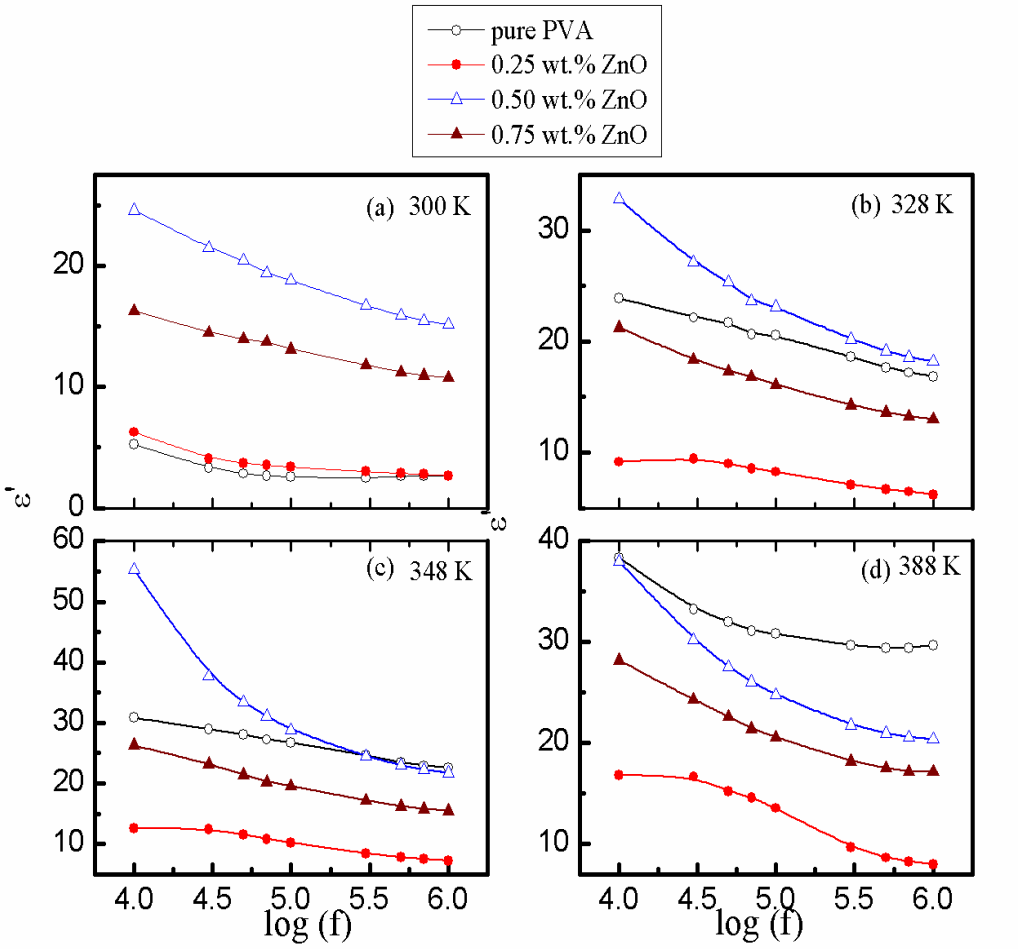

Fig. 5

Fig. 5: Frequency dependence of ε' for pure PVA film and PVA films loaded with 0.25, 0.50 and 0.75 *wt.%* ZnO-doped PVA at different temperatures: (a) 300 K, (b) 328 K , (c) 348 K and (d) 388 K.

It is also worth notable that the magnitude of ε' increases with the addition of ZnO to PVA matrix around room temperature may due to the increase in localization of charge carriers density. The sample of 0.50 wt.% ZnO-doped PVA exhibits a higher ε' at $T \leq 348$ K compared with that of other investigated samples (see Fig. 6). As seen from Fig. 6, ε' decreased with increasing f and the composite of 0.50 wt.% ZnO-doped PVA showed the highest value of ε' among the studied composite films.

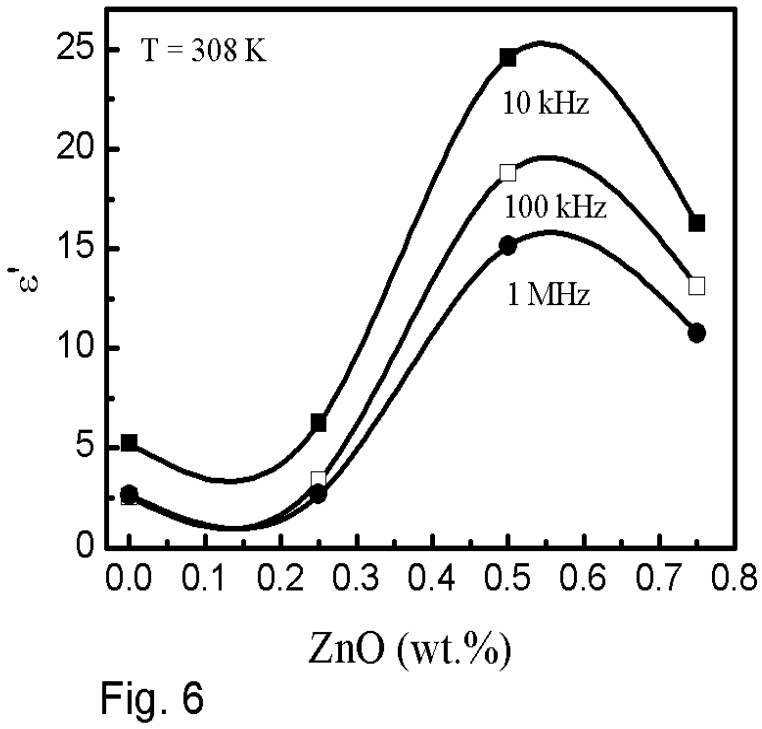

Fig. 6

Fig. 6: The variation of ε' versus the concentration of ZnO (x wt.%) nanoparticles at some selected frequencies and T = 308 K.

The temperature dependence of ε' for pure and composite samples at some fixed frequency is shown in Fig. 7(a-d). It was noticed that ε' increases with increasing temperature until T approaches $T_{\alpha c}$. By other words, a peak around $T_{\alpha c} \sim 363$ K for pure PVA was identified as due to the crystalline region or α_c-relaxation within the studied frequency range. This peak became broad and shifted a little bit to higher temperature with increasing frequency in agreement with earlier report[19]. By adding ZnO nanoparticles to the PVA matrix, the dielectric constant ε' increases up to x(wt.%) = 0.50 and then decreases. Also, $T_{\alpha c}$ peak became sharp at $f \leq 50$ kHz by adding ZnO nanoparticles compared with that of pure PVA. Although this peak became broad with increasing frequency, its position changes slightly with increasing temperature. Once

again, the sample of 0.50 wt.%-doped PVA shows a higher ε' at low frequency compared with that of pure PVA and PVA mixed with different ratios of ZnO nanoparticles.

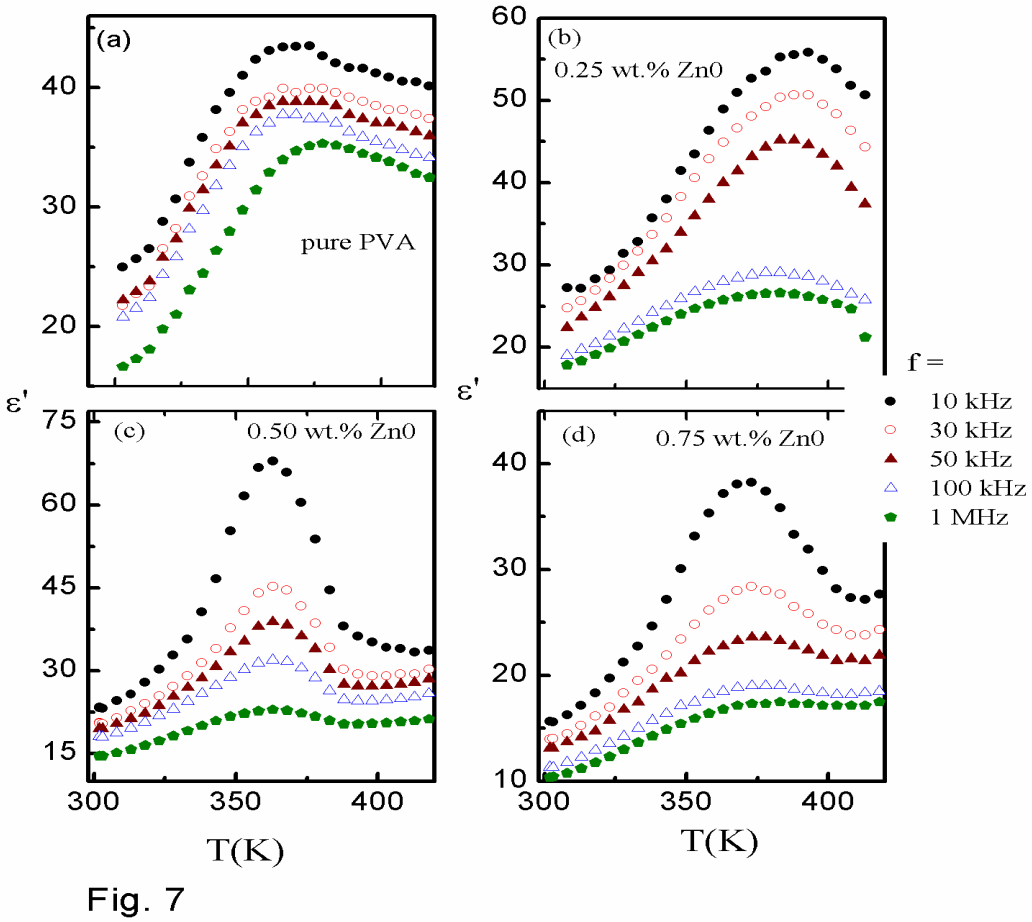

Fig. 7

Fig. 7: Temperature dependence of ε' for pure PVA film and PVA films loaded with 0.25, 0.50 and 0.75 wt.% ZnO-doped PVA at different frequencies.

A common feature of dielectric materials is frequency dependent conductivity, as given by the well known universal dynamic response [35].

$$\sigma_t = \sigma_{dc} + \sigma'(f) \qquad (4)$$

$$\sigma' = \sigma_t - \sigma_{dc} = 2\pi B f^s \qquad (5)$$

where σ_{dc} is the dc (or low frequency), conductivity, σ_t is the total conductivity, s is the universal exponent, and B is a pre-exponential factor.

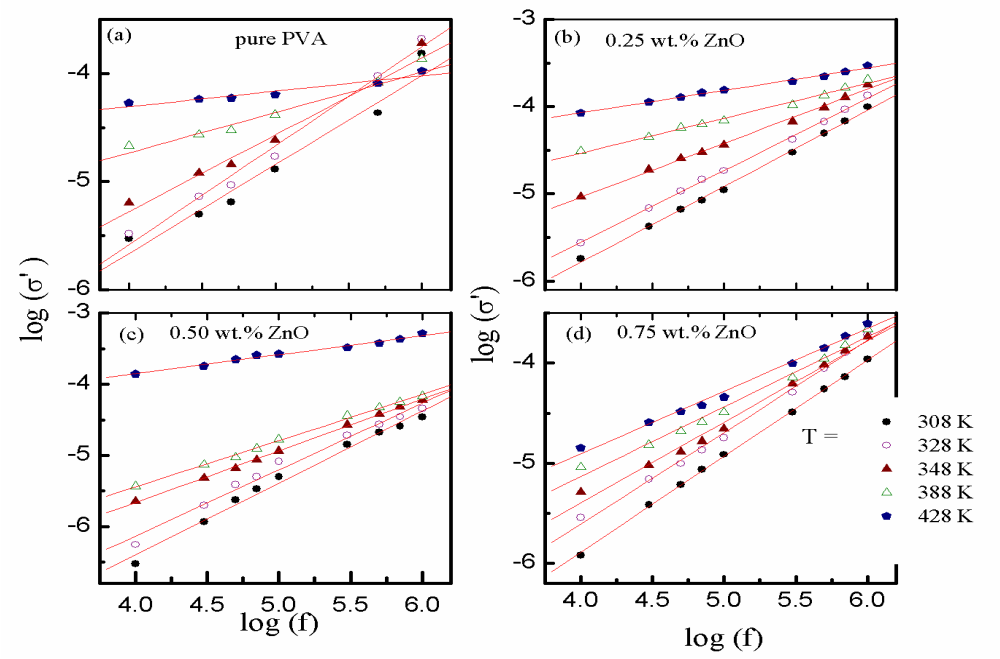

Fig. 8: Frequency dependence of σ' for pure PVA and PVA mixed with ZnO nanoparticles at different temperatures. The solid red lines are the fitting accord. to Eq. 5.

The dc conductivity was subtracted from σ_t using the low frequency region and by extrapolating σ_t to the f→0. Fig. 8(a-d) shows the variation of the real part of the ac conductivity, σ_{ac}, of some investigated samples. A linear behavior was observed between log(σ') and log(f) within the frequency (10 kHz-1 MHz) and temperature (308-428 K) ranges studied. The frequency dependence of the ac conductivity was found to be best fitted by Eq. 5, yielding the values of s. The values of s were less than unity and decreased with increasing temperature as seen in Fig. 10, in agreement with those observed for many hopping systems [36-38]. This suggests that the correlated barrier hopping (CBH) was dominant mechanism for the conduction.

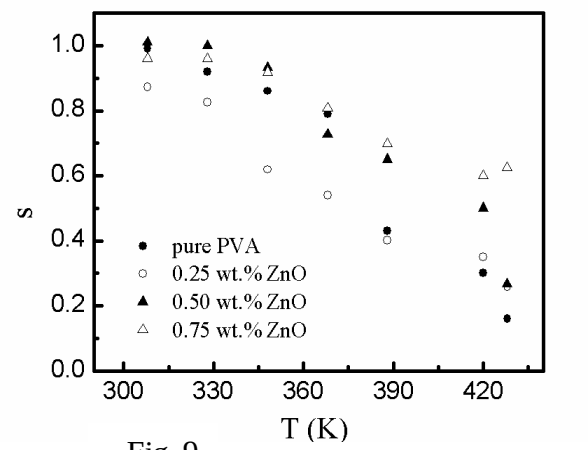

Fig. 9

Fig. 9: The variation of the frequency exponent, *s*, versus temperature for pure PVA and PVA loaded with ZnO nanoparticles.

4. Conclusion

ZnO having an average particle size 26 nm was successfully prepared using a sol-gol method and loaded into pure PVA at 0.25, 0.50 and 0.75 wt.%. SEM images showed that prepared films of pure PVA and PVA loaded with ZnO nanoparticles were homogeneous. XRD analysis indicated that the crystal structure of ZnO is hexagonal and PVA exhibited a typical semi-crystalline structure. The original structure of the ZnO nanoparticles remains unaltered in the PVA matrix. The DSC results showed that the ZnO nanoparticles reduced the thermal stability and crystallinity of the PVA. The dielectric constant, ε', exhibited a maximum value at $T \leq 328$ K for the sample of 0.50 wt.% ZnO–doped PVA. The frequency dependence of the ac conductivity revealed that the CBH was the most probable conduction mechanism for the investigated samples. It can be suggested that the ratio of 0.50/99.5 of ZnO/PVA is an optimum composite for applications.

References

1) L. Beecroft, C. K. Ober, Chem. Mater. **9**, 1302 (1997).
2) R. V. Kumar, R. Elgamiel, Y. Diamant Y and A. Gedanken, Langmuir **17**, 1406 (2001).
3) D. M. Fernandes, A. A. W. Hechenleitner, S. M. Lima, L. H. C. Andrade, A. R. L. Caires, and E. A. G. Pineda, Mater. Chem. Phys. **128**, 371 (2011).
4) M. F. Parveen, S. Umapathy, V. Dhanalakshmi, and R. Anbarasan, J. Appl. Poly. Sci. **118**, 1728 (2010).
5) Y. Lou, M. Liu, X. Miao, L. Zhang, and X. Wang, Polym. Comp.**31**, 1184 (2010).
6) F. R. Lamastra, A. Bianco, A. Meriggi, G. Montesperelli, F. Nanni, and G. Gusmano, Chem. Eng. J. **145**, 169 (2008).
7) N. Bouropoulos, G. C. Psarras, N. Moustakas, A. Chrissanthopoulos, and S. Baskoutas, Phys. Stat. Sol. (a) **205**, 2033 (2008).
8) W. E. Mahmoud, and A. A. Al-Ghamdi, Polym. Int. **59**, 1282 (2010).
9) M. S. Augustine, P. P. Jeeju, V. G. Sreevalsa, and S. Jayalekshmi, J. Phys. Chem. Solids **73**, 396 (2012).
10) D. Bhadra, J. Sannigrahi, B. K. Chaudhuri, and H. Sakata, Polym. Comp. 33, 436 (2012).
11) C. V. Chanmal, and J. P. Jog, eXPRESS Polym. Lett. 2, 294 (2008).
12) S. Mu, D. Wu, S. Qi, and Z. Wu, J. Nanomaterials 2011, Article ID 950832, 10 pages, (2011).
13) C. H. Cholakis, W. Zingg, and M. V. Seffon, J. Biomed. Mater. Res. 23, 417 (1989).
14) E. Sheha, H. Khoder, T. S. Shanap, M. G. El-Shaarawy, M. K. El Mansy, Optik 123, 1161 (2012).
15) S. B. Kondawar, S. D. Bompilwar, V. S. Khati, S. R.Thakre, V. A. Tabhane, D. K. Burghate, Archives of Applied Science Research 2, 247 (2010).
16) M. Huang, S. Mao, H. Feick, H. Yan, Y. Wu, H. Kind, E. Weber, R. Russo, P. Yang, Science 292, 1897 (2001).
17) R. Könenkamp, R. C. Word, and C. Schlegel, Appl. Phys. Lett. 85, 6004 (2004).
18) R. Tripathi, A. Kumar, C. Bharti, and T. P. Sinha, Current Appl. Phys. 10, 676 (2010).
19) F. H. Abd El-Kader, W. H. Osman, K. H. Mahmoud, M. A. F. Basha, Physica B 403, 3473 (2008).
20) B. Wunderlich, Thermal Analysis of Polymeric Materials, Springer, Berlin, (2005).
21) M. Pattabi, B. S. Amma, and K. Manzoor, Mater. Res. Bull. 42, 828 (2007).
22) I. Esparza, M. Paredes, R. Martinez, A. Gaona-Couto, G. Sanchez-Loredo, L. M. Flores-Velez, and O. Dominguez, Mater. Sci. Appl. 2, 1584 (2011).

23) A. S. Roy, S. Gupta, S. Sindhu, A. Parveen, and P. C. Ramamurthy, Composites: Part B 47, 314 (2013).
24) S. Gandhi, N. Nagalakshmi, I. Baskaran, V. Dhanalakshmi, M. R. Gopinathan Nair, and R. Anbarasan, J. Appl. Polym. Sci.118, 1666 (2010).
25) L. Jiang, X-P. Shen, J-L. Wu, and K-C. Shen, J. Appl. Polym. Sci. 118, 275 (2010).
26) X. M. Sui, C. L. Shao, Y. C. Liu, Appl. Phys. Lett. 87, 113115 (2005).
27) M. Xiong, G. Gu, B. You, and L. Wu, J. Appl. Polym. Sci. 90, 1923 (2003).
28) R. F. Bhajantri, V. Ravindrachary, A. Harisha, V. Crasta, S. P. Nayak, and B. Poojary, Polym. 47, 3591 (2006).
29) H. M. Zidan, Polym. Test.18, 449 (1999).
30) Z. I. Ali, F. A Ali, and A. M. Hosam, Spectrochimica Acta Part A 72, 868 (2009).
31) A. Hassen, A. M. El Sayed, W. M. Morsi, and S. El-Sayed, J. Appl. Phys. 112, 093525 (2012).
32) M. Y. F. Elzayat, S. El-Sayed, H. M. Osman, and M. Amin, Polym. Eng. Sci. 52, 1945 (2012).
33) N. A. Peppas, E. W. Merrill, J. Appl. Polym. Sci. 20, 1457 (1976).
34) A. N. Frone, D. M. Panaitescu, D. Donescu, C. I. Spataru, C. Radovici, R. Trusca, and R. Somoghi, BioResources 6, 487(2011).
35) A. K. Jonscher, Dielectric Relaxation in Solids, Chelsea Dielectric Press, London (1983) p.340.
36) O. G. Abdullah, S. A. Hussen, A. Alani, Asian Trans. Sci. Technol. 1, 1 (2011).
37) A. M. Saleh, R. D. Gould, A. K. Hassan, Phys. Status Solidi A 139, 379 (1993).
38) R. Bahri , H. P. Singh, Thin Solid Films 62, 291 (1979).